scientific reports

Check for updates

OPEN

Adaptive control of cardiac rhythms

Gabriel da Silva Lima[1], Marcelo Amorim Savi[2] & Wallace Moreira Bessa[3]✉

Cardiac rhythms are related to heart electrical activity, being the essential aspect of the cardiovascular physiology. Usually, these rhythms are represented by electrocardiograms (ECGs) that are useful to detect cardiac pathologies. Essentially, the heart activity starts in the sinoatrial node (SA) node, the natural pacemaker, propagating to the atrioventricular node (AV), and finally reaching the His-Purkinje complex (HP). This paper investigates the control of cardiac rhythms in order to induce normal rhythms from pathological responses. A mathematical model that presents close agreement with experimental measurements is employed to represent the heart functioning. The adopted model comprises a network of three nonlinear oscillators that represent each one of the cardiac nodes, connected by delayed couplings. The pathological behavior is induced by an external stimulus in the SA node. An adaptive controller is proposed acting in the SA node considering an strategy based on the signal obtained by the natural pacemaker and its regularization. The incorporation of adaptive compensation in a Lyapunov-based control scheme allows the compensation for the unknown dynamics. The controller ability to deal with interpatient variability is evaluated by assuming that the heart model is not available to the controller design, being used only in the simulator to assess the control performance. Results show that the adaptive term can reduce the control effort by around 3% while reducing the tracking error by 20%, when compared to the conventional feedback approach. Additionally, the controller can avoid abnormal rhythms, turning the ECG closer to the expected normal behavior and preventing critical cardiac responses. Therefore, this work demonstrates that an adaptive controller can be used to regulate the ECG signal without prior information about the system and disregarding inter- and intrapatient variability.

Keywords Adaptive control, Cardiac rhythms, Heart dynamics, Natural pacemaker, Nonlinear systems

The electrocardiogram (ECG) is one of the most common signals used to represent electrical activity of the heart, especially due to its non-invasive characteristics. It can be very useful in analyzing the cardiac system inferring heartbeat rate and regularity as well as capturing both normal and pathological behaviors. During the cardiac functioning, waves representing the electrical impulses from different areas of the heart are registered, as shown in the Fig. 1a for a normal cycle. Its physiological functioning can be understood as a complex network of self-excitatory elements, with the initial excitation occurring in the SA node, the natural pacemaker, and propagating as a wave, stimulating atria. Upon reaching the AV node, a pulse, that excites the bundle of His and, afterward, the Purkinje fibers, is initiated. The fibers distribute the stimulus to the myocardial cells, causing the ventricles contraction. From a normal ECG, Fig. 1a, three important components should be pointed out: P wave, QRS complex and T wave. P wave represents the atrium activation just after the impulse generated by the SA node. The QRS complex is formed by ventricular contraction. T wave reflects ventricular repolarization when cardiac cells return to state in which they are ready to react to another stimulus.

Mathematical models are widely employed to describe the heart dynamics, being useful for different purposes. The Hodgkin–Huxley equations, for instance, are employed to emulate the flow of ions through the cellular membrane[1,2], and although this model is capable of representing physiological phenomena at the cellular level, a population of thousands of cells would be necessary for small-scale simulations, which would require a high computational cost. In this regard, it is important to mention the pioneer work of van der Pol and van der Mark that employed a nonlinear oscillator (vdP) to represent the macroscopic behavior of heart functioning[3]. Grudzinski and Zebrowski[4] proposed a modified van der Pol (VdP) oscillator capable of presenting a more suitable description of the natural pacemaker. Afterward, Dos Santos et al.[5] modeled the cardiac dynamics

[1]Turku Intelligent Embedded and Robotic Systems Lab, Faculty of Technology, University of Turku, Turku, Finland. [2]Center for Nonlinear Mechanics, COPPE Mechanical Engineering, Universidade Federal do Rio de Janeiro, Rio de Janeiro, Brazil. [3]Smart Systems Lab, Department of Mechanical and Materials Engineering, University of Turku, Turku, Finland. ✉email: wallace.moreirabessa@utu.fi

(a)

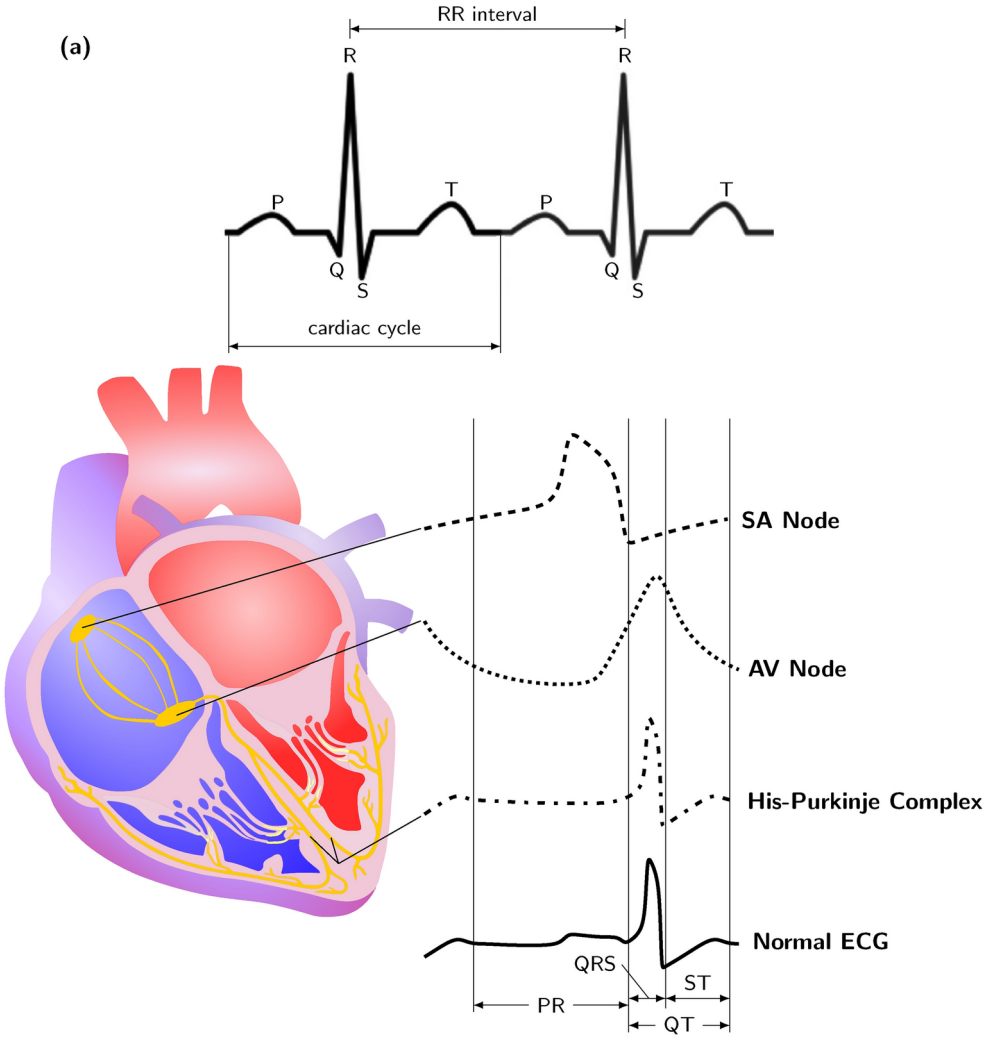

(b)

SA node		AV node		HP complex		Couplings		Time delays	
α_{SA}	3	α_{AV}	3	α_{HP}	7	$k_{SA\text{-}AV}$	3	$\tau_{SA\text{-}AV}$	0.8
ν_{SA_1}	1	ν_{AV_1}	0.5	ν_{HP_1}	1.65	$k_{AV\text{-}HP}$	55	$\tau_{AV\text{-}HP}$	0.1
ν_{SA_2}	-1.9	ν_{AV_2}	-0.5	ν_{HP_2}	-2	$k^{\tau}_{SA\text{-}AV}$	3		
d_{SA}	1.9	d_{AV}	4	d_{HP}	7	$k^{\tau}_{AV\text{-}HP}$	55		
e_{SA}	0.55	e_{AV}	0.67	e_{HP}	0.67				

Null parameters for all cases are omitted.

Figure 1. (**a**) Schematic view of the heart, including the distinct waveforms for the corresponding specialized cells, and a normal ECG; (**b**) cardiac system parameters.

considering two asymmetrically coupled modified vdP oscillators, representing the behavior of the two cardiac pacemakers, namely, the SA and AV nodes.

Gois and Savi[6] proposed a three-coupled oscillator model taking into account not only the SA and AV nodes, but also the His-Purkinje complex (HP). This reduced order model is able to capture the main features of heart dynamics represented by electro-cardiogram (ECG). Each oscillator is based on the model due to Grudzinski and Zebrowski considering bidirectional and asymmetric time-delayed couplings to represent the time spent on impulse transmissions. Cheffer et al.[7] improved the three-coupled oscillator model considering different coupling terms. The parameters associated with the model proposed by Cheffer et al.[7] are presented in the table shown in Fig. 1b. In addition, non-deterministic aspects were incorporated by considering random connections among oscillators[8–10]. Recently, Fonkou and Savi[11] introduced Duffing-type connections, which increase even more the model capability to describe the heart dynamics. It should be pointed out that these models are complex enough to emulate the dynamics of the cardiac system and simple enough to be computationally implemented.

In view of potential applications in rhythm management devices, such as artificial pacemakers and implantable cardioverter-defibrillators, the control of cardiac dynamics has been investigated by means of

different approaches. Garfinkel et al.[12,13] presented the first experiment of chaos control on biomechanical systems, applying OGY method[14] on rabbit cardiac muscle. Ferreira et al.[15] employed time-delayed feedback control for natural pacemaker using a model proposed by reference[6]. Afterward, Ferreira et al.[16] employed the same technique for ECG signals built with a three-coupled oscillators. Results showed stabilization of unstable periodic orbits embedded in chaotic attractors, avoiding critical situations. Lounis et al.[17] applied a high-order control method to the model proposed by Quiroz-Juarez et al.[18], considering the stabilization of a desired unstable periodic orbit (UPO). Khan and Nigar[19] proposed a Lyapunov-based active controller considering the combination of projective synchronization in fractional-order chaotic system with disturbance and uncertainty. Lima et al.[20] employed feedback linearization combined with neural networks in order to regulate the ECG signal by applying its signal directly at the HP complex, but without guarantees that the overall heart dynamics would be controlled as well.

The controller design represents a major challenge, as it must deal with all nonlinearities inherent in the cardiac system, as well as modeling inaccuracies and external disturbances. State observers can handle the first task[21] but may not be a suitable choice for the other issues. In this regard, adaptive approaches are suitable to compensate model uncertainties and disturbances[22–27].

This paper deals with the adaptive control of cardiac rhythms. Heart dynamics is represented by a reduced-order model considering a three-oscillator model with delayed coupling terms[6,7]. The control scheme is proposed by means of the feedback linearization approach with adaptive compensation applied to the SA node and allowing direct regularization of the natural cardiac pacemaker. In this regard, rather than directly regularizing the ECG by applying the control signal to the HP complex as described in previous work[20], the proposed approach enables immediate correction of the natural cardiac pacemaker behavior. By targeting the SA node, the controller can minimize unnecessary stimulation of other areas of the heart, affecting only the focus of the mismatched heart rhythm, consequently reducing the risk of arrhythmias or other adverse effects associated with excessive pacing, and avoiding dangerous side effects, which makes the controller application more reliable. It should be pointed out that instead of controlling heartbeat frequency[24,28,29], the proposed controller aims to regulate the ECG that can be considered as the essential measurement of the cardiac functioning dynamics. The boundedness and convergence properties of the control error are proven by means of the Lyapunov stability theory. The adaptive approach minimizes the computational complexity of the controller, making it light enough to be deployed in cardiac rhythm management devices without decreasing the controller efficiency. Furthermore, assuming that the mathematical model is not available to the control system design (it is only used to simulate the cardiac response to the control signal), the compensator is able to continuously approximate the cardiac dynamics, denoting the capacity of the proposed scheme to deal with nonlinear systems. This contribution can be understood as a proof of concept to avoid heart diseases by employing an adaptive controller that is able to compensate unknown dynamics and disturbances while dealing with within-patient and among-patient variability.

Mathematical modeling

The electrical activity of the cardiac system can be modeled from nonlinear oscillators that represent the essential heart nodes. Each node can be described by a modified Van der Pol oscillator as proposed by Grudziński and Żebrowski[4], since its dynamical response presents typical characteristics as limit cycle, synchronization and chaos[6]:

$$\ddot{u} + \alpha\, \dot{u}(u-\nu_1)(u-\nu_2) + \frac{u(u+d)(u+e)}{d\,e} = F(t) \tag{1}$$

where u stands for the electrical activity, the dot is the notation for the time derivative; α defines the pulse shape, i.e., characterizes the time when the heart receives the stimulus; ν_1 and ν_2 determine the signal amplitude, preserving the self-excitatory nature when $\nu_1\nu_2 < 0$; d and e are related to the diastolic period; $F(t)$ represents the external stimulus.

A reduced-order model of the heart electrical activity can be modeled from the coupling of three nonlinear oscillators representing SA node, AV node and HP complex[6,7]. Asymmetrical and bidirectional connections are employed in order to build a general model that is capable to reproduce the electrical activity of the heart that represents either normal or pathological functioning. Besides, the connections use time-delayed terms to represent the transmitting time spent among each one of the oscillators. On this basis, time delay reflect the signal propagation, which is similar to reaction-diffusion models[30].

Another reduced-order representation is related to external stimuli employed to capture spatiotemporal aspects. Note that external stimulus is an non-autonomous representation, which actually increases the system dimension by introducing an explicit time dependence based on spatiotemporal information. On this basis, an harmonic stimulus, $F_m(t) = \rho_m \sin(\omega_m t)$, can be employed motivated by mechanisms of fibrillation, which are represented by periodic behavior[31,32]. Under these assumptions, central nervous system stimuli are represented by self-excited behavior while external stimulus refers to situations different of the normal functioning.

Therefore, the cardiac system is governed by a reduced-order model that employs time-delayed couplings of three nonlinear oscillators and external stimuli, expressed by the following equations[9]:

$$\begin{aligned}\ddot{u}_{\mathrm{SA}} = {} & F_{\mathrm{SA}}(t) - \alpha_{\mathrm{SA}}\, \dot{u}_{\mathrm{SA}}(u_{\mathrm{SA}} - \nu_{\mathrm{SA}_1})(u_{\mathrm{SA}} - \nu_{\mathrm{SA}_2}) - \frac{u_{\mathrm{SA}}(u_{\mathrm{SA}} + d_{\mathrm{SA}})(u_{\mathrm{SA}} + e_{\mathrm{SA}})}{d_{\mathrm{SA}}\, e_{\mathrm{SA}}} + \\ & - k_{\mathrm{AV-SA}}\, u_{\mathrm{SA}} + k^{\tau}_{\mathrm{AV-SA}}\, u_{\mathrm{AV}}^{\tau_{\mathrm{AV-SA}}} - k_{\mathrm{HP-SA}}\, u_{\mathrm{SA}} + k^{\tau}_{\mathrm{HP-SA}}\, u_{\mathrm{HP}}^{\tau_{\mathrm{HP-SA}}}\end{aligned} \tag{2}$$

$$\ddot{u}_{\mathrm{AV}} = F_{\mathrm{AV}}(t) - \alpha_{\mathrm{AV}}\,\dot{u}_{\mathrm{AV}}(u_{\mathrm{AV}} - \nu_{\mathrm{AV}_1})(u_{\mathrm{AV}} - \nu_{\mathrm{AV}_2}) - \frac{u_{\mathrm{AV}}(u_{\mathrm{AV}} + d_{\mathrm{AV}})(u_{\mathrm{AV}} + e_{AV})}{d_{\mathrm{AV}}\,e_{\mathrm{AV}}} + \\ - k_{\mathrm{SA-AV}}\,u_{\mathrm{AV}} + k^{\tau}_{\mathrm{SA-AV}}\,u^{\tau_{\mathrm{SA-AV}}}_{\mathrm{SA}} - k_{\mathrm{HP-AV}}\,u_{\mathrm{AV}} + k^{\tau}_{\mathrm{HP-AV}}\,u^{\tau_{\mathrm{HP-AV}}}_{\mathrm{HP}} \tag{3}$$

$$\ddot{u}_{\mathrm{HP}} = F_{\mathrm{HP}}(t) - \alpha_{\mathrm{HP}}\,\dot{u}_{\mathrm{HP}}(u_{\mathrm{HP}} - \nu_{\mathrm{HP}_1})(u_{\mathrm{HP}} - \nu_{\mathrm{HP}_2}) - \frac{u_{\mathrm{HP}}(u_{\mathrm{HP}} + d_{\mathrm{HP}})(u_{\mathrm{HP}} + e_{\mathrm{HP}})}{d_{\mathrm{HP}}\,e_{\mathrm{HP}}} + \\ - k_{\mathrm{SA-HP}}\,u_{\mathrm{HP}} + k^{\tau}_{\mathrm{SA-HP}}\,u^{\tau_{\mathrm{SA-HP}}}_{\mathrm{SA}} - k_{\mathrm{AV-HP}}\,u_{\mathrm{HP}} + k^{\tau}_{\mathrm{AV-HP}}\,u^{\tau_{\mathrm{AV-HP}}}_{\mathrm{AV}} \tag{4}$$

Noting that indexes m and n represent SA, AV or HP, with $m \neq n$, equation terms and coefficients can be explained as follows: k_{m-n} and k^{τ}_{m-n} are coupling coefficients between m and n nodes; $x_i^{\tau_{m-n}} = x_i(t - \tau_{m-n})$ are delayed terms, where τ_{m-n} is the time delay.

The ECG can be represented by incorporating the signals of the three oscillators, being expressed as a linear combination of the state variables[6]:

$$x = \mathrm{ECG} = \beta_0 + \beta_1\,u_{\mathrm{SA}} + \beta_2\,u_{\mathrm{AV}} + \beta_3\,u_{\mathrm{HP}} \tag{5}$$

with β_0, β_1, β_2 and β_3 being parameters, so that the derivative of the ECG with respect to t becomes

$$\dot{x} = \frac{d}{dt}(\mathrm{ECG}) = \beta_1\,\dot{u}_{\mathrm{SA}} + \beta_2\,\dot{u}_{\mathrm{AV}} + \beta_3\,\dot{u}_{\mathrm{HP}} \tag{6}$$

Equations (5) and (6) can be used to represent the ECG phase space, favoring a qualitative assessment of cardiac cycle.

Since governing equations are presented in dimensionless form, it is interesting to define a dimensional time $\bar{t}$[s]: $\bar{t} = \beta_t t$, where β_t can be estimated by the ratio between real RR interval, $\mathrm{RR}_{\mathrm{exp}}$, and numerical RR interval, $\mathrm{RR}_{\mathrm{num}}$, $\beta_t = \mathrm{mean}(\mathrm{RR}_{\mathrm{exp}})/\mathrm{mean}(\mathrm{RR}_{\mathrm{num}})$.

Cardiac rhythms

In order to assess the model ability to represent cardiac dynamics, the normal rhythm is investigated. Afterward, pathological behaviors are induced by considering an external stimulus acting on the natural pacemaker (SA node). Therefore, parameters of the external stimulus $F_{\mathrm{SA}}(t)$ are modified in order to identify some pathological behaviors. It is worthy of mention that this approach for inducing aberrant cardiac dynamics is not unique. The oscillator and coupling parameters could also be changed in order to achieve similar results[7,8,33]. The choice to change the parameters of the external stimulus at the SA node is due to the characteristics of the natural pacemaker inducing the overall heart dynamics, considering that the parameters used are for a unidirectional connection[7]. The dynamical model is numerically implemented in C++ using the fourth order Runge-Kutta method with sampling rate of 1 kHz. Model parameters are presented in the table shown in Fig. 1b. Numerical results are presented in Figs. 2, 3, 4, comparing with the real ECG data provided by the PhysioNet Databases[34,35]. In order to obtain a close agreement between the experimental and simulated data, the dimensional time is scaled to reproduce a normal ECG with heart rate in approximately 90 beats per minute (bpm), which corresponds

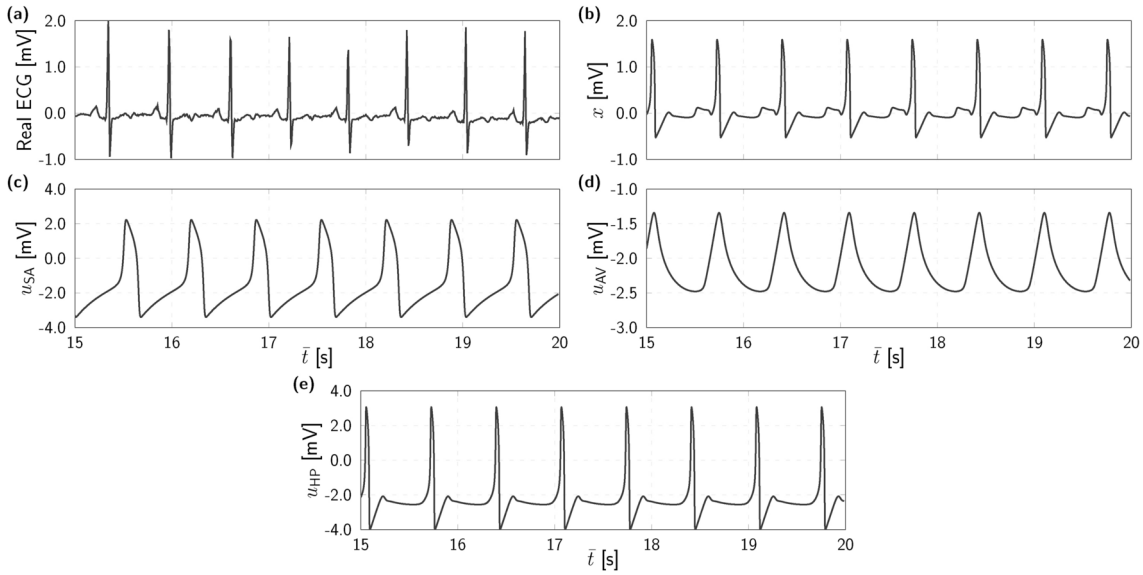

Figure 2. Normal cardiac rhythm: (**a**) real ECG signal[34,35]; (**b**) simulated time series; (**c**) SA, (**d**) AV, and (**e**) HP components of the simulated ECG.

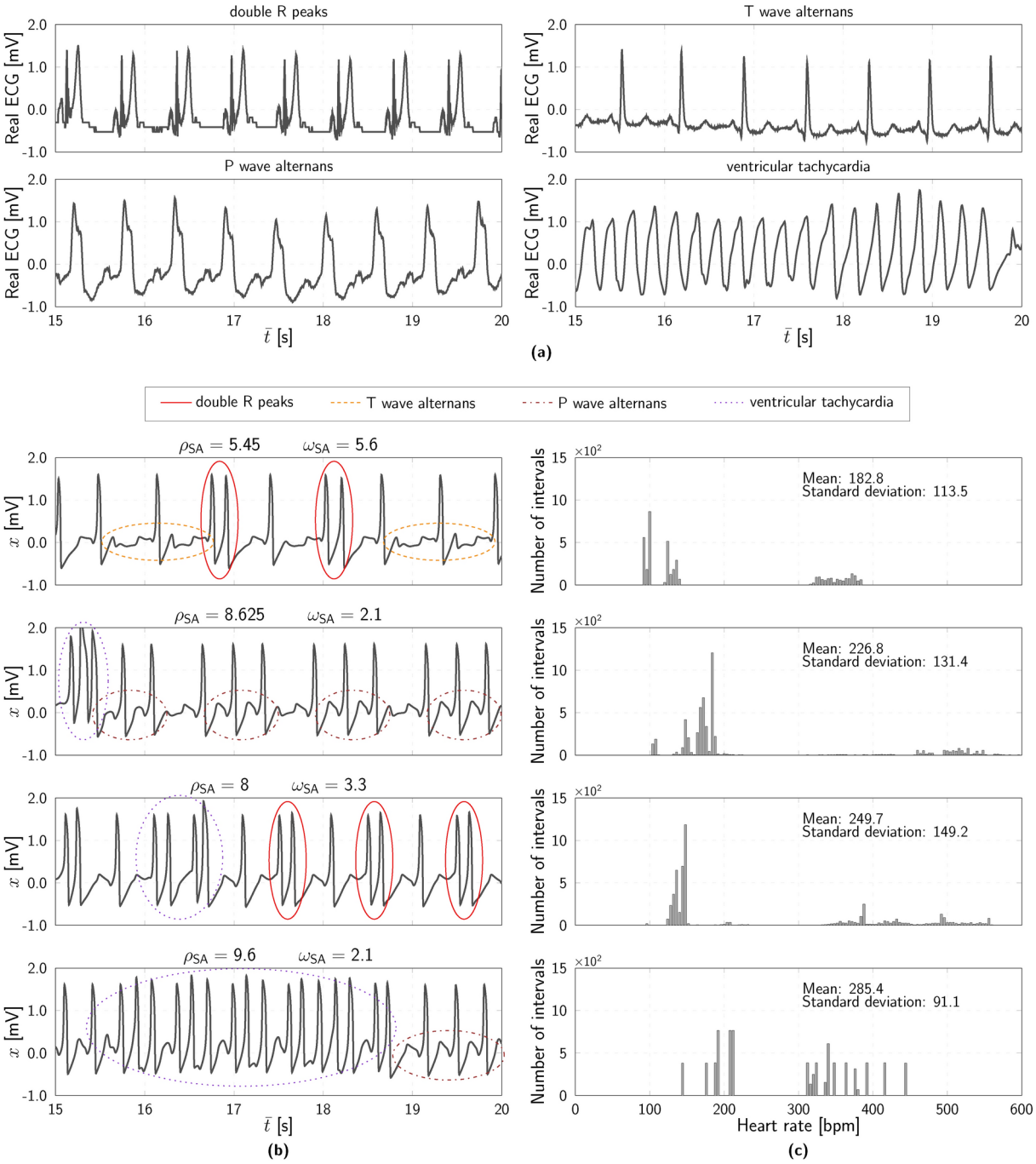

Figure 3. Pathological cardiac rhythms: (**a**) real ECG signals[34,35]; (**b**) simulated ECG signals; (**d**) histogram of the heart rate for each external stimulus.

to $\beta_t = 0.1048$. For all simulations, it is considered that $\beta_0 = 1$ mV, $\beta_1 = 0.06$, $\beta_2 = 0.1$, and $\beta_3 = 0.3$. Initial conditions are defined as $\boldsymbol{u}_0 = [-0.1, -0.6, -3.3]^\top$ and $\dot{\boldsymbol{u}}_0 = [0.025, 0.1, 2/3]^\top$, with $\boldsymbol{u} = [u_{\mathrm{SA}}\ u_{\mathrm{AV}}\ u_{\mathrm{HP}}]^\top$.

Although the general representation considers the bidirectional coupling among all the three nodes, a normal heart functioning presents unidirectional coupling starting in the SA node and being propagated to the AV node to finally reach the HP complex. For this reason, only the coupling terms related this unidirectional transmission are adopted.

The normal heart rhythm is presented in Fig. 2 showing a close agreement between the real ECG signal and the simulated one, respectively Fig. 2a and b. It should be pointed out that simulations capture the main features of the real ECG signal, characterized by P, QRS and T waves. The Fig. 2c–e show the individual components of the ECG signal related to each node.

Pathological behaviors are represented by four pathologies, with real data presented in Fig. 3a[34,35]: double R peaks; T wave alternans; P wave alternans; ventricular tachycardia. The double R peaks are associated with

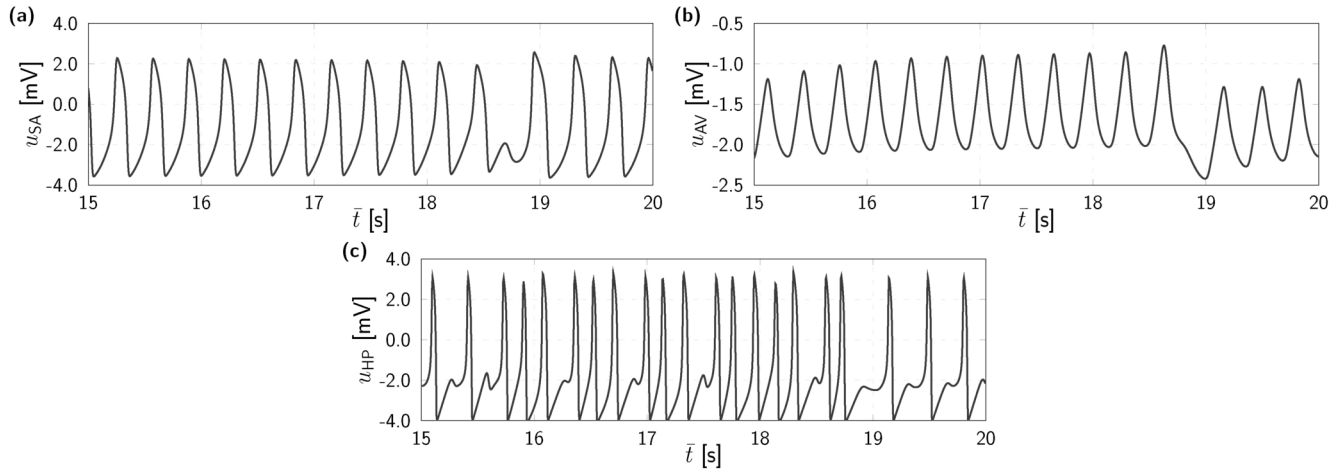

Figure 4. Components of the simulated ECG of the pathological behavior for $\rho_{SA} = 9.6$ and $\omega_{SA} = 2.1$: (**a**) SA node; (**b**) AV node; (**c**) HP complex.

branch blocks[36], which are related to delays in the transmission of the heart electrical impulses. The alternation of T waves usually indicates cardiac sudden death[37]. In the case of P wave alternans, it is possible infer junctional tachycardia[38], a form of tachycardia with the involvement of the AV node. The last pattern is the ventricular tachycardia, associated with high-frequency ventricular contraction.

Numerical simulations are carried out considering changes of the amplitude and frequency of the external stimulus of the SA node. Four combinations of these parameters are sufficient to identify these pathological ECG patterns. Figure 3b shows synthetic ECG associated with these pathological rhythms. An interesting point to be highlighted is regarding the cardiac frequency and its distribution. Different from the normal rhythm, which the heart rate can vary between 70 bpm[39] and 90 bpm[40], the pathologies presented in Fig. 3c show the heart operating in a high-frequency rate and highly dispersed.

Considering, for instance, the external excitation parameters being $\rho_{SA} = 9.6$ and $\omega_{SA} = 2.1$, the Fig. 4 shows the correspondent components of each node. As consequence of the external stimulus, the oscillation frequency of the SA signal is increased and, due to the coupling terms, both AV and HP signals are dramatically changed when compared to the normal behavior. The combination of these signals produces the pathological rhythm as depicted in the ECG signal in the Fig. 4.

Now, in order to turn these pathological rhythms into normal ones, an adaptive controller is introduced in the next section.

Adaptive controller

Heart dynamics is a spatiotemporal and multiphysics phenomenon, but the corresponding electrical activity can be described by nonlinear delayed differential equations (DDEs), which constitute a reduced-order model for the description of cardiac rhythms. However, although its description from coupled oscillators represents a simplification of the process, it can be very useful for different purposes, such as the design of control schemes. Therefore, in view of the design of a control system for the heart dynamics and considering the SA node as responsible in propagating the pathological behavior throughout the heart, the mathematical model is rewritten in the following form

$$\ddot{u}_{SA} = f + v + p \tag{7}$$

where f represents the vector field corresponding to Eq. (2), v is the control signal, assumed to be applied to the SA node, p stands for unmodeled dynamics and occasional perturbations, while $(u_{SA}, \dot{u}_{SA})$ are the states to be controlled.

Following the feedback linearization approach, the control law for a system represented by Eq. (7) can be designed as follows:

$$v = -\hat{f} - \hat{p} + \ddot{u}^{d}_{SA} - 2\lambda\dot{\tilde{u}}_{SA} - \lambda^2\tilde{u}_{SA} \tag{8}$$

with $\hat{f}$ and $\hat{p}$ being, respectively, estimated for f and p, $\tilde{u}_{SA} = u_{SA} - u^{d}_{SA}$ representing the tracking error associated with the desired state u^{d}_{SA}, and λ being a strictly positive constant.

Applying the control law (8) to (7) and assuming that all modeling uncertainties are properly represented by d, i.e. $f = \hat{f}$ is well known, the following is reached

$$\ddot{\tilde{u}}_{SA} + 2\lambda\dot{\tilde{u}}_{SA} + \lambda^2\tilde{u}_{SA} = \tilde{p} \tag{9}$$

with $\tilde{p} = p - \hat{p}$ being the approximation error.

Now, by defining a combined error signal inspired by the sliding mode method $s = \dot{\tilde{u}}_{\mathrm{SA}} + \lambda \tilde{u}_{\mathrm{SA}}$, the closed-loop dynamics (9) becomes

$$\dot{s} + \lambda s = \tilde{p} \tag{10}$$

From (10) it can be seen that in the case of perfect estimation, i.e. $\hat{p} = p$, the combined error s and therefore the tracking error $\tilde{u}$ converges to zero. Otherwise, closed-loop dynamics is driven by the approximation error $\tilde{p}$.

Therefore, an adaptive function $\hat{p}$ can be used to estimate p with any desired degree of accuracy ϵ, i.e. $p = \hat{p}^* + \epsilon$, with $\hat{p}^*$ being the optimal estimate and $|\epsilon| \leq \varepsilon$.

The boundedness and convergence properties of the closed-loop signals in the presence of modeling inaccuracies can be investigated by means of a Lyapunov-like stability analysis. Thus, let a positive-definite function V be defined as

$$V(t) = \frac{1}{2}s^2 + \frac{1}{2\eta}\delta^2 \tag{11}$$

where η is a strictly positive constant and $\delta = \hat{p} - \hat{p}^*$, with $\hat{p}^*$ being the optimal estimation that minimizes the approximation error.

Since $\dot{\delta} = \dot{\hat{p}}$, the time derivative of V becomes

$$\begin{aligned}
\dot{V}(t) &= s\dot{s} + \eta^{-1}\delta\dot{\hat{p}} \\
&= s[\tilde{p} - \lambda s] + \eta^{-1}\delta\dot{\hat{p}} \\
&= s[p - \hat{p} - \lambda s] + \eta^{-1}\delta\dot{\hat{p}} \\
&= s[\hat{p}^* + \epsilon - \hat{p} - \lambda s] + \eta^{-1}\delta\dot{\hat{p}} \\
&= -s[\lambda s - \epsilon + \delta] + \eta^{-1}\delta\dot{\hat{p}} \\
&= -s[\lambda s - \epsilon] + \eta^{-1}\delta[\dot{\hat{p}} - \eta s]
\end{aligned}$$

Hence, by updating $\hat{p}$ according to $\dot{\hat{p}} = \eta s$, $\dot{V}$ becomes

$$\dot{V}(t) = -[\lambda s - \epsilon]s \leq -[\lambda|s| - \varepsilon]|s| \tag{12}$$

Equation (12) implies that the bounds of $\hat{p}$ cannot be guaranteed when $|s| \leq \varepsilon/\lambda$. To overcome this issue, the projection algorithm[41] can be evoked to ensure that $\hat{p}$ remains within a convex region $\mathscr{D} = \{\hat{p} \in \mathbb{R}^n : |\hat{p}| \leq \mu\}$:

$$\dot{\hat{p}} = \begin{cases} \eta s & \text{if } |\hat{p}| < \mu \text{ or} \\ & \text{if } |\hat{p}| = \mu \text{ and } \eta s\hat{p} < 0 \\ 0 & \text{otherwise} \end{cases} \tag{13}$$

where μ is the desired upper bound of $|\hat{p}|$.

Since $|\hat{p}(0)| \leq \mu$, it follows that $|s| \leq \varepsilon/\lambda$ and $|\hat{p}| \leq \mu$ as $t \to \infty$. Hence, remembering that $s = \dot{\tilde{u}}_{\mathrm{SA}} + \lambda \tilde{u}_{\mathrm{SA}}$, the following condition is defined:

$$-\lambda^{-1}\varepsilon \leq \dot{\tilde{u}}_{\mathrm{SA}} + \lambda \tilde{u}_{\mathrm{SA}} \leq \lambda^{-1}\varepsilon \tag{14}$$

Thus, multiplying (14) by $e^{\lambda t}$ gives

$$-\lambda^{-1}\varepsilon\, e^{\lambda t} \leq \frac{d}{dt}\left(\tilde{u}_{\mathrm{SA}} e^{\lambda t}\right) \leq \lambda^{-1}\varepsilon\, e^{\lambda t} \tag{15}$$

Integrating (15) between 0 and t yields

$$-\frac{\varepsilon}{\lambda^2}e^{\lambda t} - \left[|\tilde{u}_{\mathrm{SA}}(0)| + \frac{\varepsilon}{\lambda^2}\right] \leq \tilde{u}_{\mathrm{SA}} e^{\lambda t} \leq \frac{\varepsilon}{\lambda^2}e^{\lambda t} + \left[|\tilde{u}_{\mathrm{SA}}(0)| + \frac{\varepsilon}{\lambda^2}\right] \tag{16}$$

By dividing (16) by $e^{\lambda t}$

$$-\frac{\varepsilon}{\lambda^2} - \left[|\tilde{u}_{\mathrm{SA}}(0)| + \frac{\varepsilon}{\lambda^2}\right] e^{-\lambda t} \leq \tilde{u}_{\mathrm{SA}} \leq \frac{\varepsilon}{\lambda^2} + \left[|\tilde{u}_{\mathrm{SA}}(0)| + \frac{\varepsilon}{\lambda^2}\right] e^{-\lambda t} \tag{17}$$

it follows, for $t \to \infty$, that

$$-\frac{\varepsilon}{\lambda^2} \leq \tilde{u}_{\mathrm{SA}} \leq \frac{\varepsilon}{\lambda^2} \tag{18}$$

Applying (18) to (14), it can be verified that

$$-2\frac{\varepsilon}{\lambda} \leq \dot{\tilde{u}}_{\mathrm{SA}} \leq 2\frac{\varepsilon}{\lambda} \tag{19}$$

Therefore, it is possible to conclude that the controller ensures the exponential convergence of the tracking error to the closed region $\mathscr{U} = \{(\tilde{u}_{\mathrm{SA}}, \dot{\tilde{u}}_{\mathrm{SA}}) \in \mathbb{R}^2 : |\tilde{u}_{\mathrm{SA}}| \leq \varepsilon\lambda^{-2} \text{ and } |\dot{\tilde{u}}_{\mathrm{SA}}| \leq 2\varepsilon\lambda^{-1}\}$.

The block diagram showed in Fig. 5 illustrates the general framework of the proposed controller. The states measured from the heart and their correspondent desired states are used to compute the tracking error. These errors are applied in the control law and utilized to compute the estimation of the unknown dynamics. This adaptive term is added into the control law and send to the heart.

Rhythm control

The proposed controller is now evaluated by numerical simulations using a sampling rate of 100 Hz. The desired states are extracted from a expected normal heart cycle, which means that the controller's main goal is to achieve a normal rhythm while avoiding pathological behavior. On this basis, the pathology investigated is related the most critical condition showed in Fig. 3: $\rho_{\mathrm{SA}} = 9.6$ and $\omega_{\mathrm{SA}} = 2.1$. Figure 6 shows the obtained results.

The controller parameter is set to $\lambda = 3$. Assuming that no prior knowledge about the heart model is available to the control system design, i.e. $\hat{f} = 0$, the ability of $\hat{p}$ to handle all neglected dynamical effects as well as the within-patient and between-patient variability is investigated. The adaptive term is initialized as $\hat{p} = 0$ and updated according to (13), with a learning rate $\eta = 300$. It is worth mentioning that the conventional controller used in comparative analysis is easily obtained by setting the learning rate to zero, which completely eliminates the adaptive contribution to the control law.

Figure 6 shows a comparison between conventional, i.e. when the adaptive compensation is removed by set $\eta = 0$, and adaptive schemes applied to the control of the pathology. As can be seen, the proposed approach is able to stabilize the expected normal rhythm in the SA node, Fig. 6b, while the conventional one fails, Fig. 6a. As consequence of the normalization of the SA signal, the adaptive controller, Fig. 6d, regulates the ECG signal converting in the a normal rhythm with clearly identification of the P, QRS and T waves and decreasing the heart rate to around 90 bpm, while with the conventional controller, Fig. 6c, in the ECG can be observed double R peaks, which indicates abnormal functioning of the heart. It should also be noted that the proposed scheme drastically reduces the control error, Fig. 6e, by 20% in the integral of absolute error (IAE) when compared with the conventional scheme.

In order to exploit the potential application of the proposed controller, the control signal v, Fig. 6f, is converted into electric current. For this purpose, it is considered that an artificial pacemaker, modeled as a continuous current source, can be implemented directly in the SA node. The current I_{SA} is calculated dividing the double integration of v by the membrane resistance of the SA node, $R_m = 20\ \Omega$[42], considering an average adult. It is noticeable that the proposed scheme can improve significantly the control of the SA node signal and, consequently, regulates the ECG, without great difference in the control signal, when compared to the conventional strategy. As a matter of fact, the proposed controller slightly reduces the control signal by 2.9% in the integral of absolute control effort (IACE).

The robustness of the controller is evaluated by adding random noise to the ρ_{SA} and ω_{SA} parameters. It is assumed a null mean and three different levels of standard deviations. Results are shown in Fig. 7 showing that the controller handles the perturbation of the external stimulus parameters. Note that the desired SA node signal is tracked by the controller, Fig. 7a.1–a.3, and the ECG presents normal behavior, Fig. 7b.1–b.3.

The adaptive controller is implemented to other external stimulus configurations as represented in Fig. 3. Results are shown in Fig. 8 where it is possible to visualize that the proposed scheme is able to track the normal SA node signal, Fig. 8a.1–a.3, regulating the heart behavior as demonstrated in the ECG signals, Fig. 8b.1–b.3. The control signal is presented in Fig. 8c.1–c.3.

A distinct arrhythmia is now of concern in order to evaluate the controller capacity for critical situations. The atrial fibrillation is characterized by the existence of several atrial reentry circuits, which are developed at different times and locations within the atrial muscle, leading to disordered atrial contraction that can potentially a cerebrovascular accident (CVA). This pathology can be simulated by considering that the coupling parameter $k_{\mathrm{AV-SA}}$ has a random variation, being extracted from a Gaussian noise with null mean and standard deviation

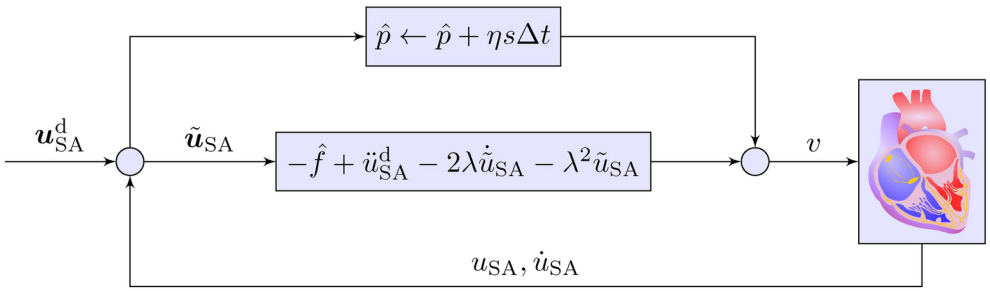

Figure 5. Block diagram of the proposed adaptive controller.

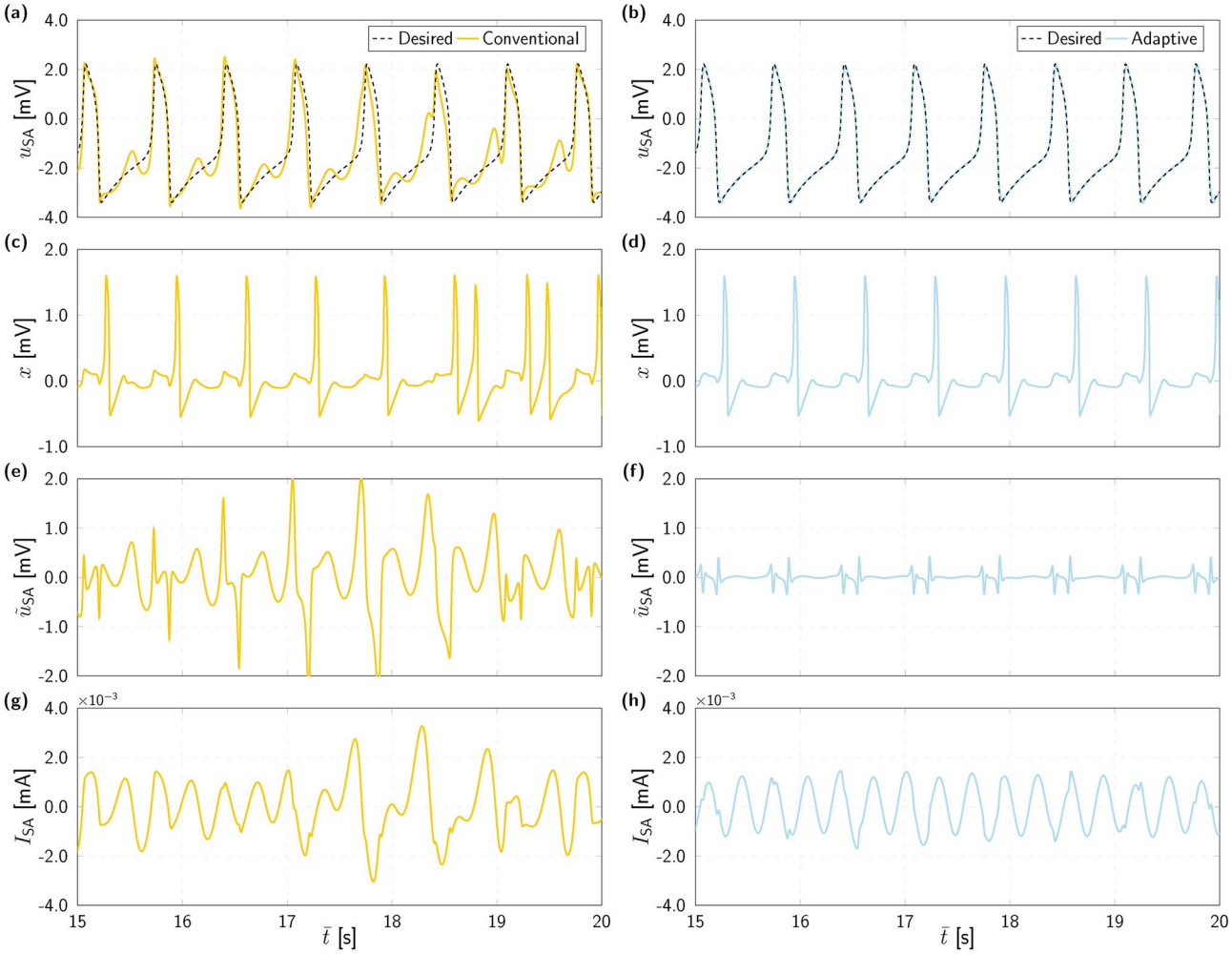

Figure 6. Simulation results: (**a**) SA node control with the conventional scheme, (**b**) SA node control with the adaptive scheme, (**c**,**d**) resulting ECG, (**e**,**f**) control error, and (**g**,**h**) control signal, for the conventional and adaptive approaches, respectively.

of 30 for each iteration. The controller is employed by using the same control parameters used to the previous cases, and the ECG is controlled by applying the control signal at the SA node. Results are presented in the Fig. 9 that shows the pathological ECG, highlighting the experimental ECG, the histogram of cardiac frequency, the trajectory tracking for the SA node, the controlled ECG and the control signal. It is noticeable that the controller is able to perform this pathological rhythm, avoiding the critical arrhythmia.

Conclusions

This paper investigates the control of the electrical activity of the heart. A mathematical model based on three coupled nonlinear oscillators is employed to describe cardiac rhythms, being able to represent both normal and pathological behaviors. From the model perspective, pathological rhythms are obtained when an external stimulus is considered in the SA node, known as the heart's natural pacemaker. In order to avoid these abnormal heart activities, an adaptive controller is proposed based on the SA node. A learning scheme designed by means of the Lyapunov stability analysis allows the adaptive term to be adjusted online. The controller performance is evaluated with computational simulations with results showing that the controller is able to perform rhythm control. Due to the coupling between the heart nodes, the stabilization of the natural pacemaker promotes the overall cardiac system to be driven to normal behavior.

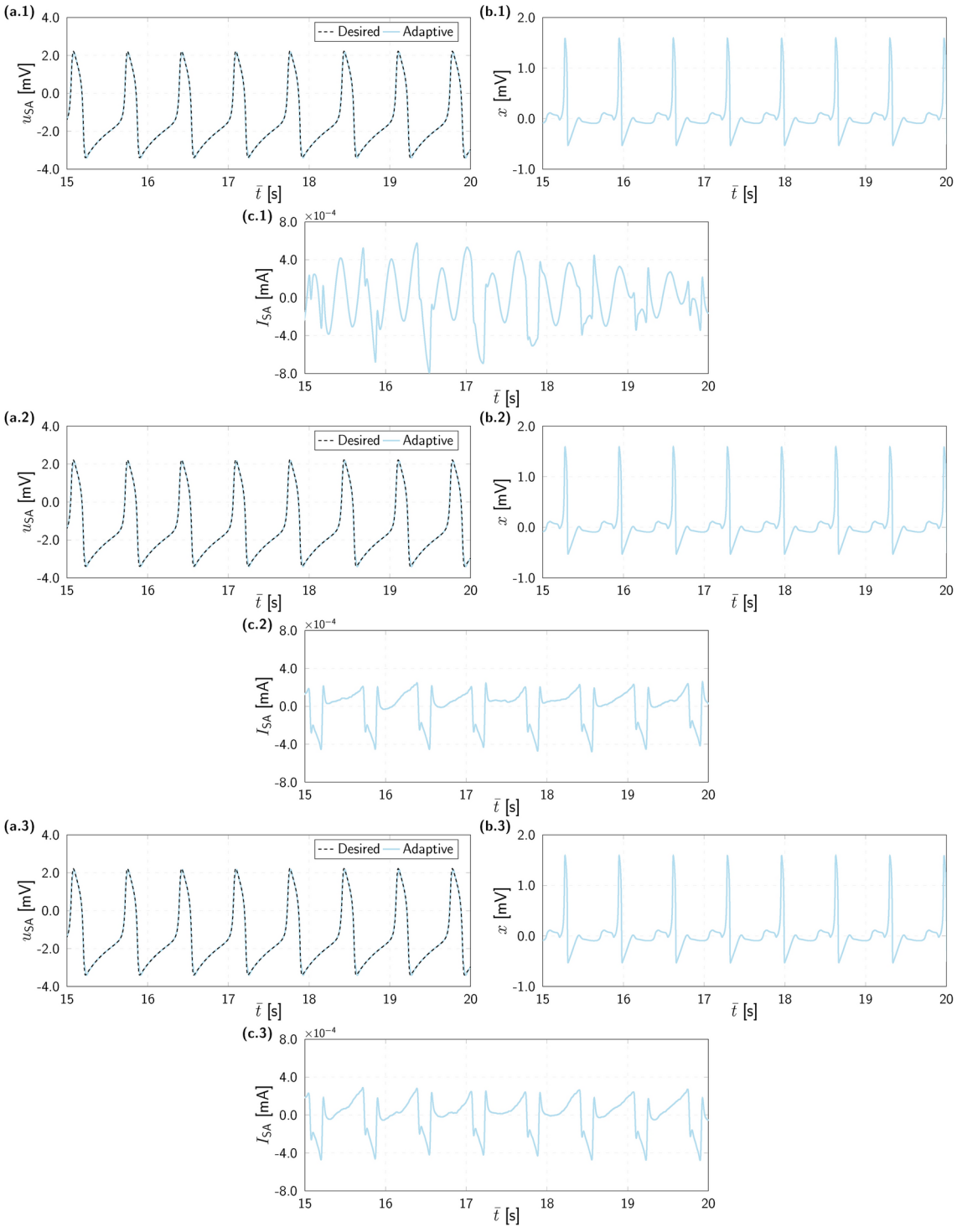

Figure 7. Simulation results: (**a**) SA node control with the adaptive scheme, (**b**) resulting ECG with the adaptive controller, (**c**) control signal, (.1) results for standard deviation of $\sigma = 0.01$, (.2) results for standard deviation of $\sigma = 0.1$, and (.3) results for standard deviation of $\sigma = 0.5$.

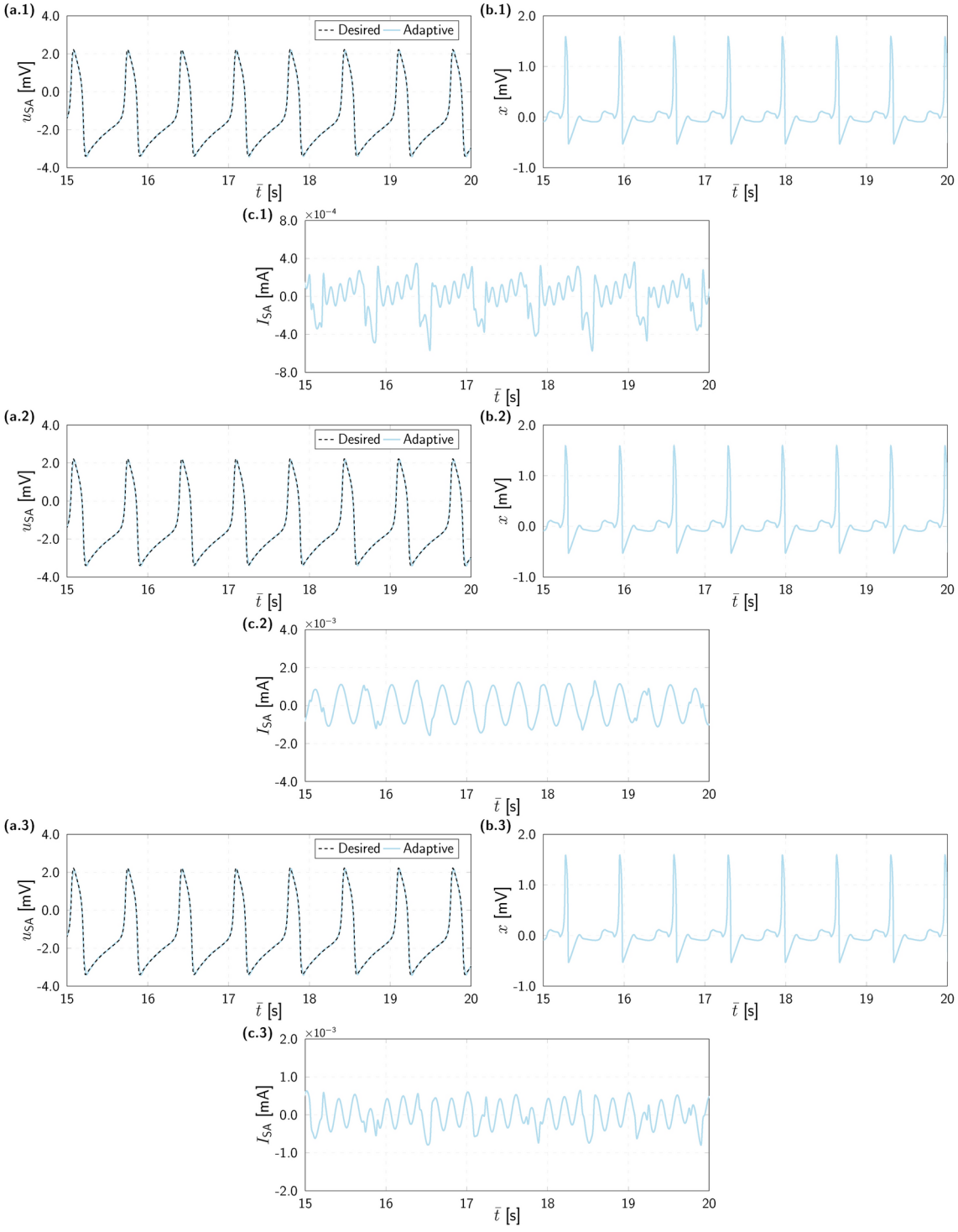

Figure 8. Simulation results: (**a**) SA node control with the adaptive scheme, (**b**) resulting ECG with the adaptive controller, (**c**) control signal, (.1) results for $\rho_{\mathrm{SA}} = 5.45$ and $\omega_{\mathrm{SA}} = 5.6$, (.2) results for $\rho_{\mathrm{SA}} = 8.625$ and $\omega_{\mathrm{SA}} = 2.1$, and (.3) results for $\rho_{\mathrm{SA}} = 8$ and $\omega_{\mathrm{SA}} = 3.3$.

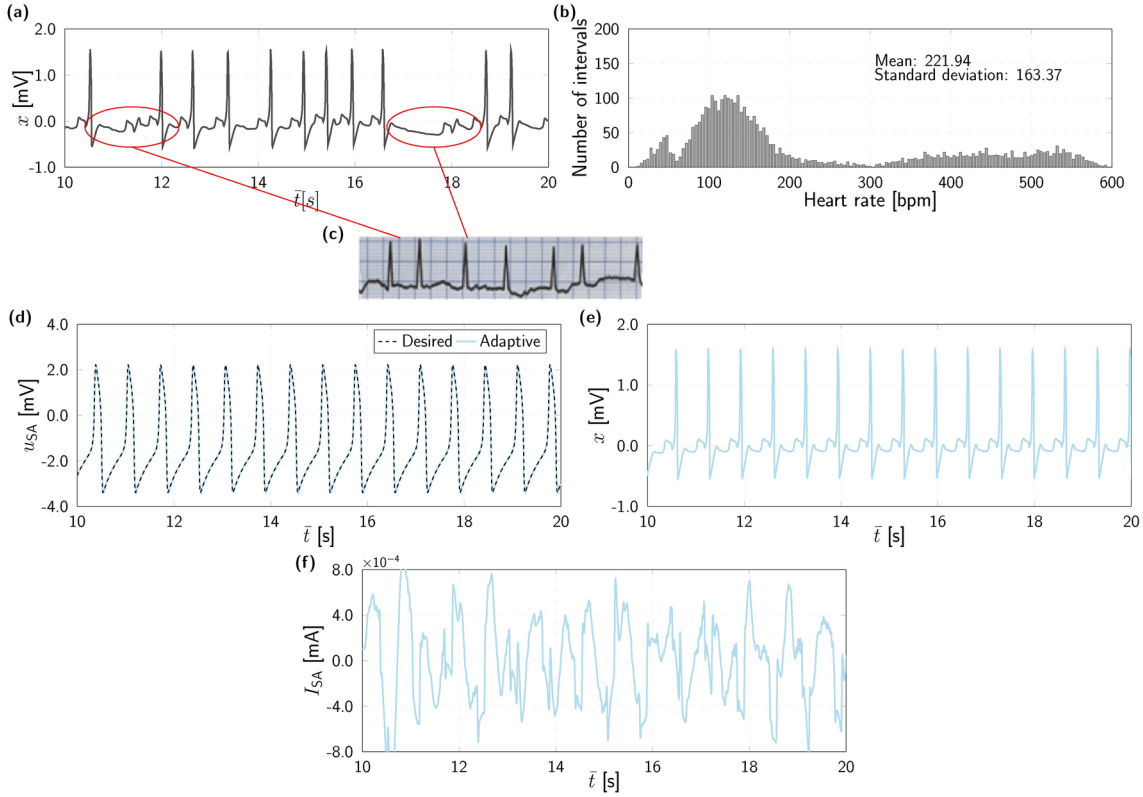

Figure 9. Simulation results for atrial fibrillation: (**a**) ECG for fibrillation, (**b**) histogram of cardiac frequency, (**c**) experimental data, (**d**) trajectory tracking for the SA node, (**e**) ECG for the controlled case, and (**f**) control signal.

Data availability

The datasets generated during the current study are available from the corresponding author on reasonable request.

Received: 25 February 2024; Accepted: 25 September 2024
Published online: 07 October 2024

References

1. Hodgkin, A. L. & Huxley, A. F. The components of membrane conductance in the giant axon of loligo. *J. Physiol.* **116**, 473 (1952).
2. McCormick, D. A., Shu, Y. & Yu, Y. Hodgkin and huxley model–still standing?. *Nature* **445**, E1–E2 (2007).
3. Van Der Pol, B. & Van Der Mark, J. Lxxii. The heartbeat considered as a relaxation oscillation, and an electrical model of the heart. *London Edinburgh Dublin Philos. Magaz. J. Sci.* **6**, 763–775 (1928).
4. Grudziński, K. & Żebrowski, J. J. Modeling cardiac pacemakers with relaxation oscillators. *Physica A* **336**, 153–162 (2004).
5. Dos Santos, A. M., Lopes, S. R. & Viana, R. R. L. Rhythm synchronization and chaotic modulation of coupled van der pol oscillators in a model for the heartbeat. *Physica A* **338**, 335–355 (2004).
6. Gois, S. R. & Savi, M. A. An analysis of heart rhythm dynamics using a three-coupled oscillator model. *Chaos Solitons Fractals* **41**, 2553–2565 (2009).
7. Cheffer, A., Savi, M. A., Pereira, T. L. & De Paula, A. S. Heart rhythm analysis using a nonlinear dynamics perspective. *Appl. Math. Model.* **96**, 152–176 (2021).
8. Cheffer, A. & Savi, M. A. Random effects inducing heart pathological dynamics: An approach based on mathematical models. *Biosystems* **196**, 104177 (2020).
9. Cheffer, A. & Savi, M. A. Analysis of cardiovascular rhythms using mathematical models. *Henry J. Cardiol. Cardiovasc. Med.* **5**, 022 (2021).
10. Cheffer, A., Ritto, T. G. & Savi, M. A. Uncertainty analysis of heart dynamics using random matrix theory. *Int. J. Non-Linear Mech.* **129**, 103653 (2021).
11. Fonkou, R. F. & Savi, M. A. Heart rhythm analysis using nonlinear oscillators with duffing-type connections. *Fractal Fractional* **7**, 592 (2023).
12. Garfinkel, A., Spano, M. L., Ditto, W. L. & Weiss, J. N. Controlling cardiac chaos. *Science* **257**, 1230–1235 (1992).
13. Garfinkel, A., Weiss, J. N., Ditto, W. L. & Spano, M. L. Chaos control of cardiac arrhythmias. *Trends Cardiovasc. Med.* **5**, 76–80 (1995).
14. Ott, E., Grebogi, C. & Yorke, J. A. Controlling chaos. *Phys. Rev. Lett.* **64**, 1196–1199 (1990).
15. Ferreira, B. B., De Paula, A. S. & Savi, M. A. Chaos control applied to heart rhythm dynamics. *Chaos Solitons Fractals* **44**, 587–599 (2011).
16. Ferreira, B. B., Savi, M. A. & De Paula, A. S. Chaos control applied to cardiac rhythms represented by ECG signals. *Phys. Scr.* **89**, 105203 (2014).

17. Lounis, F., Boukabou, A. & Soukkou, A. Implementing high-order chaos control scheme for cardiac conduction model with pathological rhythms. *Chaos Solitons Fractals* **132**, 109581 (2020).
18. Quiroz-Juárez, M. *et al.* Generation of ECG signals from a reaction-diffusion model spatially discretized. *Sci. Rep.* **9**, 1–10 (2019).
19. Khan, A. & Nigar, U. Combination projective synchronization in fractional-order chaotic system with disturbance and uncertainty. *Int. J. Appl. Comput. Math.* **6**, 1–22 (2020).
20. Lima, G. S., Savi, M. A. & Bessa, W. M. Intelligent control of cardiac rhythms using artificial neural networks. *Nonlinear Dyn.* **111**, 11543–11557 (2023).
21. Gharesi, N., Arefi, M. M., Khayatian, A. & Bahrami, Z. Extended state observer-based control of heartbeat described by heterogeneous coupled oscillator model. *Commun. Nonlinear Sci. Numer. Simul.* **101**, 105884 (2021).
22. Kitamura, T., Matsuda, K. & Akashi, H. Adaptive control technique for artificial hearts. *IEEE Trans. Biomed. Eng.* **BME–33**, 839–844 (1986).
23. Aabid, M., Elakkary, A. & Sefiani, N. Real-time cardiac monitoring through the application of an adaptive controller to human heart. *Int. Rev. Autom. Control (IREACO)* **10**, 63–71 (2017).
24. Karar, M. E. Robust rbf neural network-based backstepping controller for implantable cardiac pacemakers. *Int. J. Adapt. Control Signal Process.* **32**, 1040–1051 (2018).
25. Bessa, W., De Paula, A. S. & Savi, M. A. Adaptive fuzzy sliding mode control of a chaotic pendulum with noisy signals. *ZAMM J. Appl. Math. Mech./Zeitschrift fur Angewandte Mathematik und Mechanik* **94**, 256–263 (2014).
26. Dos Santos, J. D. B. & Bessa, W. M. Intelligent control for accurate position tracking of electrohydraulic actuators. *Electron. Lett.* **55**, 78–80 (2019).
27. Lima, Gd. S., Porto, D. R., de Oliveira, A. J. & Bessa, W. M. Intelligent control of a single-link flexible manipulator using sliding modes and artificial neural networks. *Electron. Lett.* **57**, 869–872 (2021).
28. Yadav, J., Rani, A. & Garg, G. Intelligent heart rate controller for cardiac pacemaker. *Int. J. Comput. Appl.* **36**, 22–29 (2011).
29. Mohsin, E. F., Tashan, T. & Karam, E. H. Design and fpga implementation of immune-pid controller based on bbo algorithm for heart rate regulation. *Int. J. Intell. Eng. Syst* **14**, 432–440 (2021).
30. Quiroz-Juárez, M. A. *et al.* Generation of ECG signals from a reaction-diffusion model spatially discretized. *Sci. Rep.* **9**, 19000 (2019).
31. Skanes, A. C., Mandapati, R., Berenfeld, O., Davidenko, J. M. & Jalife, J. Spatiotemporal periodicity during atrial fibrillation in the isolated sheep heart. *Circulation* **98**, 1236–1248 (1998).
32. Jalife, J., Berenfeld, O., Skanes, A. & Mandapati, R. Mechanisms of atrial fibrillation: Mother rotors or multiple daughter wavelets, or both?. *J. Cardiovasc. Electrophysiol.* **9**, S2-12 (1998).
33. Cheffer, A. & Savi, M. A. Biochaos in cardiac rhythms. *Eur. Phys. J. Spec. Top.* **231**, 833–845 (2022).
34. Goldberger, A. L. *et al.* Physiobank, physiotoolkit, and physionet: Components of a new research resource for complex physiologic signals. *Circulation* **101**, e215–e220 (2000).
35. Maršánová, L., Smíšek, R., Němcová, A., Smital, L. & Vítek, M. Brno university of technology ECG signal database with annotations of p wave (but pdb). *PhysioNet* (2021).
36. Canabrava, S. *Eletrocardiografia* (Med eLearning Cursos Interativos, 2014).
37. Barbosa, P. R. B. *et al.* Alternância elétrica da onda t: Bases eletrofisiológicas e aplicações clínicas baseadas em evidências. *Revista da SOCERJ* **17**, 227–242 (2004).
38. Brugada, P., Brugada, J., Mont, L., Smeets, J. & Andries, E. W. A new approach to the differential diagnosis of a regular tachycardia with a wide qrs complex. *Circulation* **83**, 1649–1659 (1991).
39. Hampton, J. & Hampton, J. *The ECG Made Easy E-Book: The ECG Made Easy E-Book* (Elsevier Health Sciences, 2019).
40. Haddad, S. A., Houben, R. P. & Serdijin, W. The evolution of pacemakers. *IEEE Eng. Med. Biol. Mag.* **25**, 38–48 (2006).
41. Ioannou, P. & Fidan, B. *Adaptive Control Tutorial* (SIAM, 2006).
42. Grant, A. O. & Strauss, H. C. Intracellular potassium activity in rabbit sinoatrial node. evaluation during spontaneous activity and arrest. *Circ. Res.* **51**, 271–279 (1982).

Acknowledgements

The authors would like to acknowledge the support of the Brazilian Research Agencies CNPq (Conselho Nacional de Desenvolvimento Científico e Tecnológico), CAPES (Coordenação de Aperfeiçoamento de Pessoal de Nível Superior) and FAPERJ (Fundação Carlos Chagas Filho de Amparo à Pesquisa do Estado do Rio de Janeiro) and through the INCT-EIE (National Institute of Science and Technology - Smart Structures in Engineering), CNPq, CAPES and FAPEMIG (Fundação de Amparo à Pesquisa do Estado de Minas Gerais). The support of the AFOSR (Air Force Office of Scientific Research) is also acknowledged.

Author contributions

G.S.L. M.A.S. and W.M.B. conceived the presented idea. M.A.S. proposed the mathematical model. G.S.L. and W.M.B. designed the adaptive controller. G.S.L. deployed the computer code, ran the simulations and wrote the manuscript with the support of M.A.S. and W.M.B. All authors read and approved the final manuscript.

Declarations

Competing interests

The authors declare no competing interests.

Additional information

Correspondence and requests for materials should be addressed to W.M.B.

Reprints and permissions information is available at www.nature.com/reprints.

Publisher's note Springer Nature remains neutral with regard to jurisdictional claims in published maps and institutional affiliations.